

Spin-charge separation and quantum spin Hall effect of β -bismuthene

Alexander C. Tyner¹ and Pallab Goswami^{1,2}

¹ Graduate Program in Applied Physics, Northwestern University, Evanston, Illinois, 60208, USA and

² Department of Physics and Astronomy, Northwestern University, Evanston, Illinois, 60208, USA

(Dated: September 28, 2022)

Field theory arguments suggest the possibility of \mathbb{Z} -classification of quantum spin Hall effect with magnetic flux tubes, that cause separation of spin and charge degrees of freedom, and pumping of spin or Kramers pair. However, the *proof of principle* demonstration of spin-charge separation is yet to be accomplished for realistic, *ab initio* band structures of spin-orbit-coupled materials, lacking spin-conservation law. In this work, we perform thought experiments with magnetic flux tubes on β -bismuthene to demonstrate spin-charge separation, and quantized pumping of spin for three insulating states that can be accessed by tuning filling fractions. With a combined analysis of momentum-space topology and real-space response, we identify important role of topologically non-trivial bands, supporting even integer winding numbers, which cannot be inferred from symmetry-based indicators. Our work sets a new standard for prediction of two-dimensional, quantum spin-Hall materials, based on precise bulk invariant and universal topological response.

I. INTRODUCTION

Chern insulators¹⁻³ and quantum spin Hall (QSH) insulators⁴⁻⁹ are two prominent examples of two-dimensional (2D) topological phases of matter. For crystalline materials, they respectively arise due to the existence of net Chern number ($\mathcal{C}_{GS} \in \mathbb{Z}$)^{2,3,10} and net relative or spin Chern number ($\mathcal{C}_{R,GS} \in \mathbb{Z}$)^{4,5} for completely occupied bands. The Chern number \mathcal{C}_{GS} of time-reversal-symmetry (\mathcal{T}) breaking materials describes quantized Abelian Berry flux ($2\pi\mathcal{C}_{GS}$) through 2D Brillouin zone (BZ) and it can be calculated using TKNNY formula², and by imposing twisted boundary condition (TBC) in real space¹⁰. Furthermore, the topological response (pumping of electric charge $\Delta Q = e\mathcal{C}_{GS}$) can be directly probed by inserting a magnetic flux tube carrying flux ϕ , and adiabatically tuning ϕ between 0 and $\phi_0 = h/e$ ¹.

In contrast to \mathcal{C}_{GS} , $\mathcal{C}_{R,GS}$ describes quantized, non-Abelian Berry flux $2\pi\mathcal{C}_{R,GS}$ through 2D BZ. The definition of non-Abelian Berry flux for spin-orbit-coupled materials has many subtleties due to the absence of continuous spin rotation symmetry or spin conservation law. Kane and Mele formulated \mathbb{Z}_2 -classification of QSH effect of \mathcal{T} -symmetric systems, i.e., odd vs. even integer distinction of $\mathcal{C}_{R,GS}$ ⁴. For generic \mathcal{T} -symmetric systems, the \mathbb{Z}_2 invariant $(-1)^{\mathcal{C}_{R,GS}}$ can be calculated from the gauge-invariant spectrum of Wilson loops (Wannier charge centers) of non-Abelian Berry connection¹¹⁻¹⁴. Furthermore, for inversion-symmetric materials, it can be easily identified from a symmetry-based indicator, which is the product of parity eigenvalues at time-reversal-invariant momentum points⁸.

To go beyond \mathbb{Z}_2 -classification of $\mathcal{C}_{R,GS}$ without relying on spin and momentum conservation laws, various authors have considered the role of generalized TBCs¹⁵⁻¹⁷. However, the insertion of spin-gauge flux and the implementation of spin-dependent TBC requires detailed understanding of underlying basis states and the

mechanism of violation of spin-conservation law. Hence, its application has practical limitation.

To overcome this challenge, Qi and Zhang¹⁸, and Ran *et al.*¹⁹ proposed diagnosis of \mathbb{Z}_2 QSH states with magnetic flux tubes (i.e., gauging of conserved quantity). Employing 4-band models of QSH states with $|\mathcal{C}_{R,GS}| = 1$, they have shown that a flux tube, carrying half of flux quantum $\phi = \frac{\phi_0}{2}$ (\mathcal{T} -invariant, π flux) binds two degenerate, zero-energy, mid-gap states. At half-filling, one of these modes is occupied, and the ground state exhibits 2-fold-degeneracy ($SU(2)$ -doublet). Consequently, the flux tube remains charge-neutral, and carries spin quantum number $\pm\frac{1}{2}$. When both modes are occupied (empty), the flux tube carries electric charge $-e$ ($+e$), and spin quantum number 0 ($SU(2)$ -singlets). Such states can be accessed by doping insulators with one electron (hole). This solitonic mechanism of *spin-charge separation* (SCS) is similar to what is known for polyacetylene^{20,21} and topologically ordered, correlated systems²². When \mathcal{T} is broken by generic values of ϕ , the bound modes and the half-filled ground state become non-degenerate. But the flux tube continues to bind spin and no electric charge. By adiabatically tuning ϕ from 0 to ϕ_0 , quantized pumping of spin (one Kramers-pair) can be observed [see Appendix A].

While Refs. 18 and 19 and subsequent works²³⁻²⁵ advanced conceptual understanding of QSH effect, they relied on idealized models of decoupled Chern insulators, carrying opposite Chern numbers. Due to the underlying $U(1)$ spin-rotation symmetry, these models admit \mathbb{Z} -classification of $\mathcal{C}_{R,GS} = \mathcal{C}_{GS,\uparrow} = -\mathcal{C}_{GS,\downarrow}$, and the spin-Hall conductivity $\sigma_{xy}^z = 2\mathcal{C}_{R,GS}$. The SCS for such systems would be governed by $SU(2|\mathcal{C}_{R,GS}|)$ -multiplets [see Appendix A]. Since $\mathcal{C}_{R,GS}$ for decoupled models is easily calculated, the analysis of SCS only serves academic interest.

For realistic band structures of spin-orbit-coupled materials, various crystalline-symmetry allowed hybridization terms destroy $U(1)$ spin-conservation law. Since

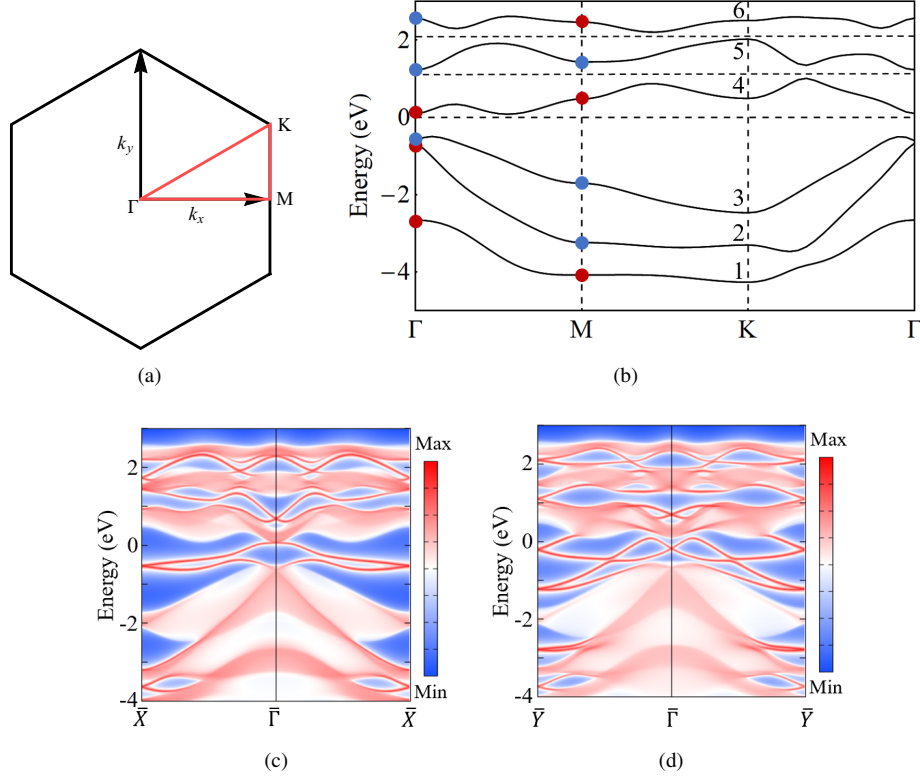


FIG. 1. (a) Hexagonal Brillouin zone of β -bismuthene. (b) Band structure along high-symmetry path $\Gamma - M - K - \Gamma$ and energies are measured with respect to a reference value $E_0 = 0$. Bands are numbered according to their energies at Γ point, such that $E_n(\Gamma) < E_{n+1}(\Gamma)$. Parity eigenvalues ± 1 at time-reversal-invariant-momentum points are denoted by red and blue dots, respectively. The dashed lines correspond to three representative values of Fermi energy, tuned in direct band gaps, leading to $1/2$ -, $2/3$ -, and $5/6$ -filled insulators. They support non-trivial \mathbb{Z}_2 -invariant $\nu_{0,GS} = 1$. (c,d) Spectral density on the surface under open boundary conditions along (c) y-axis and (d) x-axis. The mid-gap edge-modes, connecting bulk valence and conduction bands imply first-order topology of insulating states.

there is no simple theoretical framework for computing $\mathfrak{C}_{R,GS}$ of such systems, the demonstration of SCS would allow unambiguous diagnosis of $|\mathfrak{C}_{R,GS}|$ or \mathbb{N} -classification of QSH insulators. Moreover, \mathbb{Z} -classification can be accomplished by measuring spin expectation values, during the process of spin-pumping. Recently, we have addressed the stability of SCS for topologically non-trivial planes of 3D Dirac semimetals (4-band model)²⁶, and 3-fold symmetric planes (8-band model)²⁷ of octupolar topological insulators²⁸. These models support SCS respectively controlled by $SU(2)$ and $SU(4)$ multiplets. Moreover, the quantized pumping of spin occurs even in the absence spin-rotation symmetry and gapless, helical edge-states.

Encouraged by these results, in this work, we perform *proof of principle* demonstration of SCS for realistic, *ab initio* band structures. For concreteness, we focus on a single (111)-bilayer of elemental bismuth (Bi), also known as β -bismuthene, as a suitable material platform. The analysis of SCS will be guided by the calculation of gauge-invariant magnitudes of relative Chern numbers

of constituent bands ($|\mathfrak{C}_{R,n}|$ for n -th band)²⁹. Thus, the importance of \mathbb{Z}_2 -trivial bands, possessing even integer winding number ($\mathfrak{C}_{R,j} = 2s_j \neq 0$) will be critically addressed. We also present a brief contrasting study of β -antimonene, which does not exhibit SCS.

II. BAND TOPOLOGY OF BISMUTHENE

Symmetry-based topological classification of 3D Bi has dramatically evolved over past fifteen years. The band structure of Bi was initially classified as topologically trivial, with strong \mathbb{Z}_2 TI index $\nu_{0,GS} = 0$ ^{8,30}. Now it is identified as a higher-order, topological crystalline insulator with strong \mathbb{Z}_4 index $\kappa_{1,GS} = 2$ ³¹⁻³³. In contrast to this, the ground state of β -bismuthene is known to be a \mathbb{Z}_2 QSH insulator^{6,34-39}, supporting helical edge states^{6,34,35}.

The crystal structure of β -bismuthene is described by buckled honeycomb layers with space group $P6/mcc$. The material supports \mathcal{T} and space-inversion (\mathcal{P}) sym-

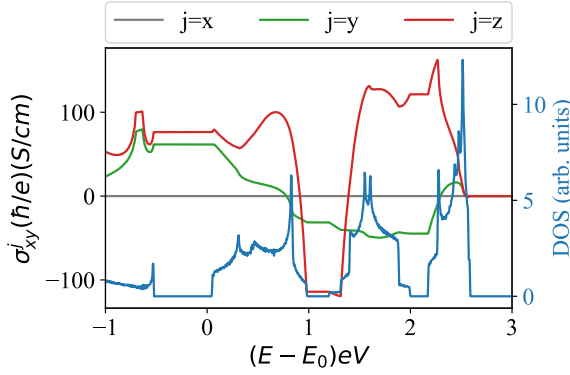


FIG. 2. Spin Hall conductivity σ_{xy}^j of β -bismuthene from first principles calculations, as a function of energy. Three insulating states can be identified from direct gaps in density of states. In addition to showing plateau-like features, σ_{xy}^z shows sharp change of sign, when bands 4 and 5 become occupied. While these results cannot capture precise topological properties, they indicate topological non-triviality of these \mathbb{Z}_2 -trivial bands.

metries, leading to the two-fold Kramers degeneracy of all energy bands throughout the hexagonal BZ of Fig. 1(a). Using the crystal structure and lattice constants from Ref. 40, the *ab initio* band structure has been calculated with Quantum Espresso^{41–43}. The band structure along high-symmetry path $\Gamma - M - K - \Gamma$ is shown in Fig. 1(b). As these bands are well separated from other bands, an accurate 12-band, Wannier tight-binding (TB) model has been constructed from $p_{x,y,z}$ orbitals from each layer. We have included spin-orbit coupling for all calculations and utilized a $40 \times 40 \times 1$ Monkhorst-Pack grid of k -points and a plane wave cutoff of 100 Ry. The model construction and topological analysis are performed with Wannier90 and Z2pack^{12,14,44}.

When the Fermi level is tuned inside direct gaps between bands (i) 3 and 4, (ii) 4 and 5, and (iii) 5 and 6, we find three insulators at filling fractions $1/2$, $2/3$, and $5/6$. From the parity eigenvalues shown in Fig. 1(b), we find that only bands 2 and 6 possess non-trivial \mathbb{Z}_2 -index $\nu_{0,n} = 1$, and all three insulators admit non-trivial \mathbb{Z}_2 -index $\nu_{0,GS} = 1$. The results of edge-states calculations, using iterative Greens function method⁴⁵ and Wannier Tools⁴⁶ are displayed in Figs. 1(d) and 1(c). All three insulators support gapless edge modes, which can cross the Fermi level 2 or 6 times³⁴. Whether $|\mathfrak{C}_{R,GS}| = 1$ or 3 cannot be determined from edge-spectrum.

It is instructive to compute spin Hall conductivity, following the current state-of-the-art of computational materials science,^{47–49} and the results are shown in Fig. 2. Due to the non-conservation of spin, this method cannot capture quantization of spin Hall effect. But it provides rough guidance for understanding qualitative properties of three insulators. Notice that σ_{xy}^z displays plateau-

Band index n	3-fold eigenvalues $C_{3,n}$	\mathbb{Z}_2 -index $\nu_{0,n}$	Relative Chern number $ \mathfrak{C}_{R,n} $
1	$e^{\pm i\frac{\pi}{3}}$	0	0
2	$e^{\pm i\frac{\pi}{3}}$	1	1
3	$e^{\pm i\frac{\pi}{3}}$	0	0
4	$e^{\pm i\pi}$	0	2
5	$e^{\pm i\frac{\pi}{3}}$	0	2
6	$e^{\pm i\pi}$	1	1

TABLE I. Natural number classification of relative Chern numbers of constituent Kramers-degenerate bands of β -bismuthene. The 3-fold rotation eigenvalues and \mathbb{Z}_2 -indices are listed for convenience. The symmetry data of rotation and parity eigenvalues are insufficient to distinguish between bands possessing $|\mathfrak{C}_{R,n}| = 0$ and 2.

like features, when E is tuned in direct band gaps, and changes sign when \mathbb{Z}_2 -trivial bands 4 and 5 become occupied. Are bands 4 and 5 topologically trivial?

This question can be conclusively answered by identifying the magnitude of relative Chern number of Kramers-degenerate bands ($|\mathfrak{C}_{R,n}|$) by computing in-plane Wilson loops of $SU(2)$ Berry connection²⁹. The results are displayed in Table I and the details of calculations are presented in Appendix B. We see that bands 4 and 5 carry even integer invariants. While they do not change odd integer classification of $\mathfrak{C}_{R,GS}$, they can change the magnitude and the sign of $\mathfrak{C}_{R,GS}$. Table I suggests the following possibilities: (i) $|\mathfrak{C}_{R,GS}| = 1$, (ii) $|\mathfrak{C}_{R,GS}| = 1, 3$, (iii) $|\mathfrak{C}_{R,GS}| = 1, 3, 5$, respectively for $1/2$, $2/3$, and $5/6$ filled insulators. While it is possible to compute signed $\mathfrak{C}_{R,n}$ by adding a small time-reversal symmetry breaking field, we will resolve uncertainties with SCS.

III. SPIN CHARGE SEPARATION

To study real-space topological response we insert a flux tube at the center of 2D system. The hopping matrix element H_{ij} connecting lattice sites \mathbf{r}_i and \mathbf{r}_j is modified to $H_{ij} e^{i\phi_{ij}}$. Working with Coulomb gauge, we define the Peierls phase factor

$$\phi_{ij} = \frac{\phi}{\phi_0} \int_{\mathbf{r}_i}^{\mathbf{r}_j} \frac{\hat{z} \times \mathbf{r}}{r^2} \cdot d\mathbf{l}. \quad (1)$$

We first perform exact diagonalization of gauged Hamiltonian for 24×24 unit cells, under periodic boundary conditions (PBC), yielding $N = 6912$ eigenstates. When the total number of electrons $N_e = \frac{N}{2}, \frac{2N}{3}, \frac{5N}{6}$, and $\phi = \phi_0/2$, we find two-fold-degenerate mid-gap states bound to the flux tube, leading to two-fold degeneracy of

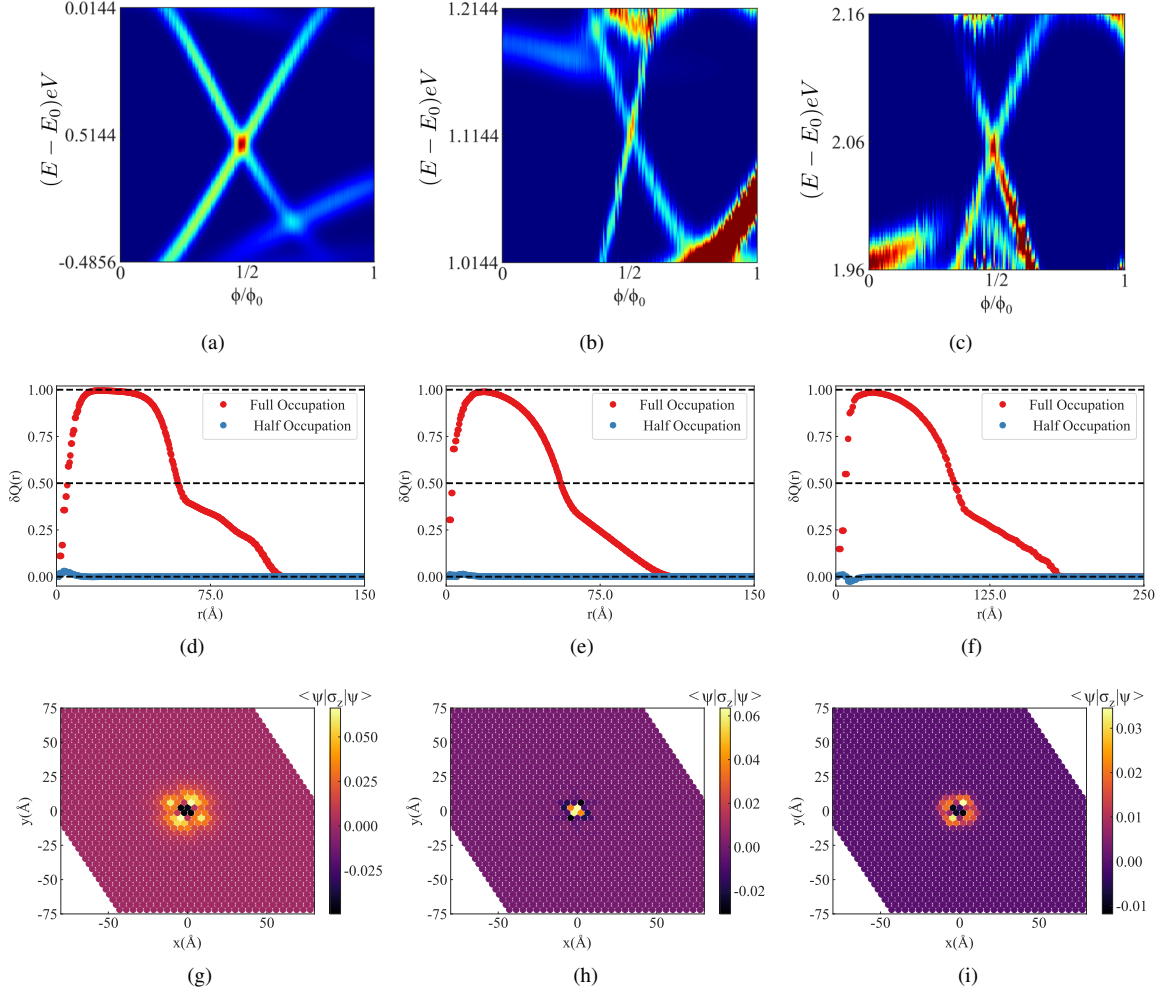


FIG. 3. Spin-charge separation in β -bismuthene. (a)-(c) Local density of states on flux tube, as a function of ϕ/ϕ_0 , with energies scanned in the vicinity of band gaps. For time-reversal-invariant flux $\phi = \phi_0/2$, two-fold degenerate bound states occur precisely at $1/2$, $2/3$, and $5/6$ filling fractions. For any generic value of flux, time-reversal-symmetry is broken and bound states become non-degenerate. As ϕ is tuned from 0 to ϕ_0 , one Kramers-pair is pumped, revealing $|\mathcal{C}_{R,GS}| = 1$ for all three insulators. Induced electric charge $\delta Q(r)$ (in units of $-e$) on flux tube, as a function of radial distance r from the flux tube, for (d) $1/2$ -filled, (e) $2/3$ -filled, (f) $5/6$ -filled insulators, with $\phi/\phi_0 = 1/2$. When the bound states are half-filled (fully occupied), the maximum value of induced charge saturates to quantized value 0 ($-e$). The results remain unchanged for $\phi/\phi_0 \neq 1/2$. The spin expectation values of unoccupied bound modes for $\phi = (\frac{1}{2} - \epsilon)\phi_0$, and $\epsilon = 10^{-3}$ for (g) $1/2$ -filled, (h) $2/3$ -filled, (i) $5/6$ -filled insulators. The profile of spin polarization for $2/3$ -filled insulator is opposite to those for $1/2$ - and $5/6$ -filled insulators.

ground states [see Figs. 3(a)-3(b)]. When $\phi \neq \phi_0/2$, flux tube breaks time-reversal-symmetry and the degeneracy of bound states (ground state) is lifted. By holding N_e fixed at commensurate values, and varying ϕ from 0 to ϕ_0 , we observe pumping of one Kramers pair.¹⁸

Next we compute the induced electric charge on flux-tube for $\phi = \phi_0/2$. This calculation is done in two steps.⁵⁰ For a given number of electrons, by summing over *all occupied states*, we evaluate the area charge densities $\sigma_1(\mathbf{r}_i, N_e)$, and $\sigma_0(\mathbf{r}_i, N_e)$, respectively in the presence and absence of flux tube. The induced charge density is defined as $\delta\sigma(\mathbf{r}_i, N_e) = \sigma_1(\mathbf{r}_i, N_e) -$

$\sigma_0(\mathbf{r}_i, N_e)$, and the total induced charge within a circle of radius r , centered at the flux tube is determined from $\delta Q(r, N_e) = \sum_{|\mathbf{r}_i| < r} \delta\sigma(\mathbf{r}_i, N_e)$. In order to achieve sufficient numerical accuracy, induced charge calculations are performed for a system size of 60×60 unit cells, yielding $N = 43,200$ eigenstates. The results are displayed in Figs. 3(d)-3(f). When $N_e = \frac{N}{2}, \frac{2N}{3}, \frac{5N}{6}$, one of the degenerate mid-gap modes is occupied (half-occupation of mid-gap states), and we find $\delta Q(r, N_e) = 0$, which remains unchanged for generic values of ϕ . For $N_e = \frac{N}{2} \pm 1, \frac{2N}{3} \pm 1, \frac{5N}{6} \pm 1$, the bound modes become completely occupied (+) and empty (−), and the max-

imum values of $\delta Q(r, N_e)$ saturate to quantized results $\mp e$, respectively.

Therefore, we can conclude that each non-trivial insulator supports $|\mathfrak{C}_{R,GS}| = 1$, which can only be consistent with the following assignments of signed relative Chern numbers

$$(\mathfrak{C}_{R,1}, \mathfrak{C}_{R,2}, \mathfrak{C}_{R,3}, \mathfrak{C}_{R,4}, \mathfrak{C}_{R,5}, \mathfrak{C}_{R,6}) = \pm(0, 1, 0, -2, +2, -1), \quad (2)$$

defined with respect to a global spin quantization axis for all bands. When bands 4 and 5 are occupied, $\mathfrak{C}_{R,GS}$ will change sign. This assertion can be further substantiated by evaluating expectation values of spin operators $\mathbb{1}_{6 \times 6} \otimes \sigma \equiv \sigma$ for bound states. We have computed expectation values for $\phi = (\frac{1}{2} - \epsilon)\phi_0$ and $\epsilon \rightarrow 0^+$, such that the bound states are infinitesimally split in energy. The expectation values for $\sigma_{x,y}$ are negligibly small. As occupied and unoccupied modes support opposite signs for $\langle \psi_n | \sigma_z | \psi_n \rangle$, we are only showing the results for unoccupied modes in Figs. 3(g)-3(i). All signs become reversed for $\phi = (\frac{1}{2} + \epsilon)\phi_0$, as a consequence of spin-pumping. Therefore, flux tube for 1/2-, 2/3-, 5/6-filled insulators respectively support +, -, + signs for $\langle \psi_n | \sigma_z | \psi_n \rangle$, when $\phi < \phi_0/2$.

IV. CONCLUSIONS

In summary, we have shown that bilayer bismuth is a suitable platform for studying spin charge separation as a universal topological response of quantum spin Hall insulators. The combined analysis of non-Abelian Berry phase in momentum space and real space topological response clearly identify non-trivial topology of bands that carry even integer winding numbers. Topology of such bands are not easily detected by symmetry-based indicators. In Appendix C we also analyze bulk topology of β -antimonene, which supports \mathbb{Z}_2 -trivial ground state. With first principles based calculations of spin Hall conductivity and insertion of magnetic flux tube we show that β -antimonene is not a quantum spin Hall insulator (i.e., $\mathfrak{C}_{R,GS} = 0$).

In this work, we have only gauged a conserved quantity (electric charge) to identify the presence or absence of spin-pumping. This can be reliably used for many candidate materials for quantum spin Hall effect. Guided by the results of this work, one can further pursue insertion of spin-gauge flux (gauging of non-conserved quantity) to demonstrate pumping of electric charge ($\delta Q = 2e\mathfrak{C}_{R,GS}$), which directly tracks signed relative/spin Chern number. Due to technical subtleties and numerical cost of such calculations, such thought experiments on real materials would be reported in a future work.

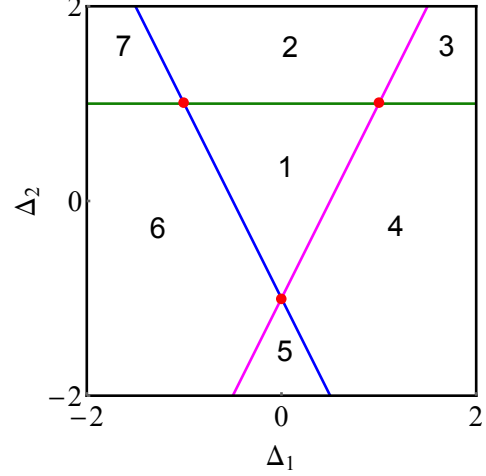


FIG. 4. Phase diagram of four-band model for $M = 1$. Parity eigenvalues and bulk winding numbers are listed in Table II. Along blue, magenta, and green lines, the bulk band gap can close at Γ , M , and X points, respectively. Red dots denote multi-critical points.

Phase	Parity eigenvalues ($\delta_\Gamma, \delta_M, \delta_X$)	$\mathfrak{C}_{R,GS}$
1	(-1, -1, -1)	0
2	(-1, -1, +1)	$2 \operatorname{sgn}(t)$
3	(-1, +1, +1)	$\operatorname{sgn}(t)$
4	(-1, +1, -1)	$-\operatorname{sgn}(t)$
5	(+1, +1, -1)	$-2 \operatorname{sgn}(t)$
6	(+1, -1, -1)	$-\operatorname{sgn}(t)$
7	(+1, -1, +1)	$\operatorname{sgn}(t)$

TABLE II. Patterns of parity eigenvalues and bulk winding numbers for various phases of Fig. 4.

Appendix A: Spin-charge separation of minimal models

Let us consider the following Bernevig-Hughes-Zhang (BHZ) model⁵ of sp hybridization on a square lattice

$$\frac{H_0(\mathbf{k})}{t} = \sum_{j=1}^3 d_j(\mathbf{k}) \Gamma_j = \sin k_x \Gamma_1 + \sin k_y \Gamma_2 + [M + \Delta_1(\cos k_x + \cos k_y) + \Delta_2 \cos k_x \cos k_y] \Gamma_3, \quad (A1)$$

where $\Gamma_1 = \tau_1 \otimes \sigma_1$, $\Gamma_2 = \tau_1 \otimes \sigma_2$, and $\Gamma_3 = \tau_3 \otimes \sigma_0$ are mutually anti-commuting matrices. The 2×2 identity matrix σ_0 (τ_0) and Pauli matrices $\sigma_{j=1,2,3}$ ($\tau_{j=1,2,3}$) operate on spin (orbital/parity) index. The hopping parameter t has units of energy, and M , Δ_1 , Δ_2 are dimensionless tuning parameters, and the lattice constant has been set to unity. The Hamiltonian anti-commutes









SU(2)-multiplets for $\mathfrak{C}_{R,GS} = \pm 1$	SU(4)-multiplets for $\mathfrak{C}_{R,GS} = \pm 2$
1. Doublet: $N_e=0, \delta Q=0$ 	1. Sextet: $N_e=0, \delta Q=0$; 6-permutations of 
2. Singlets: $N_e=+1, \delta Q=-e$  $N_e=-1, \delta Q=+e$ 	2. Singlets: $N_e=+2, \delta Q=-2e$  $N_e=-2, \delta Q=+2e$ 
	3. Quartet: $N_e=+1, \delta Q=-e$; 4-permutations of 
	4. Quartet: $N_e=-1, \delta Q=+e$; 4-permutations of 

FIG. 5. Schematic of spin-charge separation and induced quantum numbers for magnetic π flux tube. The occupation number of mid-gap states is denoted by 0 and 1. For half-filled systems, the number of added electrons $N_e = 0$, and the induced electric charge $\delta Q = 0$. By adding one electron or hole one can access $\delta Q = \mp e$ on flux tube for $\mathfrak{C}_{R,GS} = \pm 1$. Additional charge quantum numbers are found for $\mathfrak{C}_{R,GS} = \pm 2$.

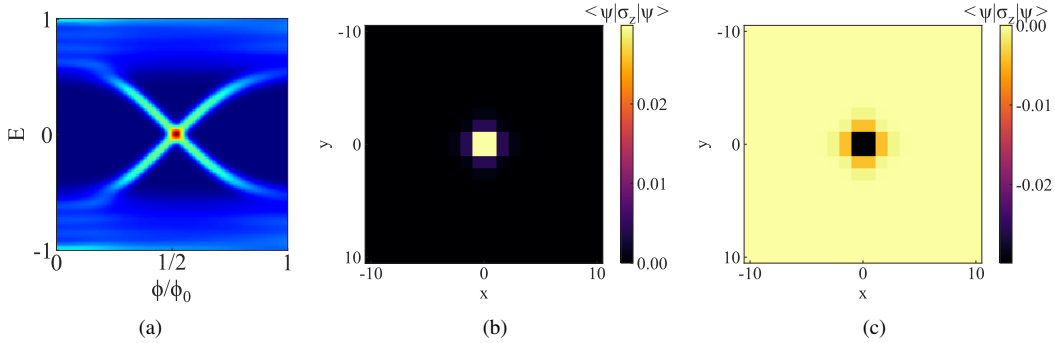


FIG. 6. Spin-charge separation for Phase 3 and Phase 4, with $t > 0$. (a) Local density of states on flux tube for both phases shows pumping of one Kramers pair. Spin expectation value $\langle \psi_n | \sigma_z | \psi_n \rangle (x, y)$ of unoccupied bound mode, when $\phi = (\frac{1}{2} - \epsilon)\phi_0$, and $\epsilon = 10^{-2}$, for (b) Phase 3, (c) Phase 4. The spin density on flux tube tracks $\text{sgn}(\mathfrak{C}_{R,GS})$.

with $\Gamma_4 = \tau_1 \otimes \sigma_3$, and $\Gamma_5 = \tau_2 \otimes \sigma_0$, and commutes with $\Gamma_{45} = [\Gamma_4, \Gamma_5]/(2i) = \sigma_3 \otimes \tau_0$. Thus, $\Psi_i^\dagger \mathbb{1} \Psi_i$ and $\Psi_i^\dagger \Gamma_{45} \Psi_i$ are generators of total number $[U_+(1)]$ and spin rotation $[U_-(1)]$ symmetries, respectively.

At time-reversal-invariant momentum points $\Gamma : \mathbf{Q} = (0, 0)$, $M : \mathbf{Q} = (\pi, \pi)$, and $X : \mathbf{Q} = \{(\pi, 0), (0, \pi)\}$ points $H_0 \rightarrow td_3(\mathbf{Q})\Gamma_3$, and $[H_0(\mathbf{Q}), \Gamma_3] = 0$. Parity eigenvalues of valence bands are given by $-\text{sgn}(d_3(\mathbf{Q}))$. A representative phase diagram is shown in Fig. 4, and the pattern of parity eigenvalues and the bulk invariant

$$\mathfrak{C}_{R,GS} = \frac{1}{4\pi} \int_{BZ} d^2k \, \hat{\mathbf{d}} \cdot \left(\frac{\partial \hat{\mathbf{d}}}{\partial k_x} \times \frac{\partial \hat{\mathbf{d}}}{\partial k_y} \right) \quad (\text{A2})$$

are listed in Table II. As phases 3, 4, 6, and 7 (2 and 5) support $|\mathfrak{C}_{R,GS}| = 1$ ($|\mathfrak{C}_{R,GS}| = 2$), magnetic π -flux tube would bind 2 (4) zero-energy bound states. Therefore, SCS would be controlled by $SU(2)$ and $SU(4)$ multiplets, respectively (see Fig. 5). When flux ϕ is tuned from 0 to ϕ_0 , one and two units of spin (Kramers-pair) would be pumped.

After Fourier transformation, we obtain tight-binding model $H_{0,ij}$ in real-space. In the presence of magnetic flux tube, placed at origin, the matrix elements $H_{0,ij}$ between different lattice sites can be replaced by $H_{0,ij}e^{i\phi_{ij}}$, with $\phi_{ij} = \frac{\phi}{\phi_0} \int_{\mathbf{r}_i}^{\mathbf{r}_j} \frac{\hat{\mathbf{z}} \times \mathbf{r}}{r^2} \cdot d\mathbf{l}$. The SCS and spin-pumping for Phases 3, 4, 6, and 7 are controlled by $SU(2)$ multiplets. In Fig. 6, we show the results

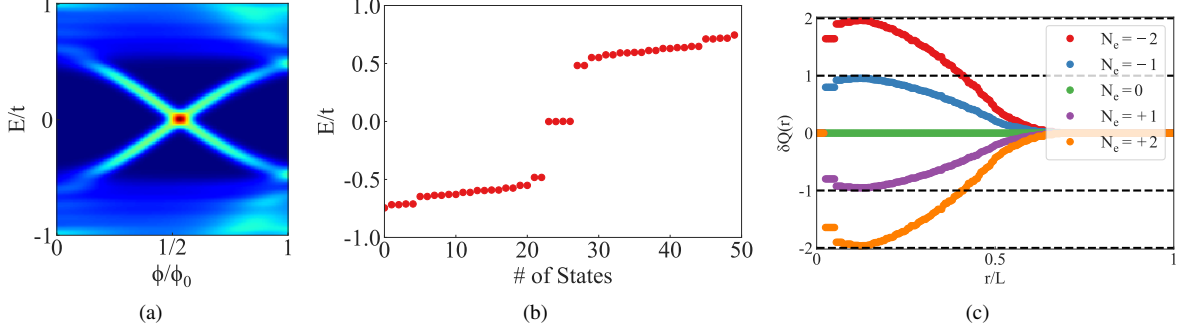


FIG. 7. Spin-charge separation for Phase 2 and Phase 5, possessing $|\mathfrak{C}_{R,GS}| = 2$. All calculations are performed for a system size of 24×24 lattice sites, under periodic boundary conditions. (a) Local density of states on flux tube as a function of ϕ/ϕ_0 . Both branches of spectra, which traverse the bulk gap are two-fold degenerate, implying pumping of two Kramers pairs. (b) At $\phi = \phi_0/2$, they lead to four zero-energy bound states, and 6-fold degeneracy of the half-filled ground state. (c) Induced electric charge (in units of $-e$) on π -flux tube within a radius r , and N_e denotes the number of doped electrons. The maximum induced charge saturates to quantized values $\pm 2e$ for the non-degenerate states ($SU(4)$ -singlets), and $\pm e$ for the four-fold degenerate states ($SU(4)$ quartets), and 0 for the half-filled state ($SU(4)$ sextet), respectively.

for Phase 3 and Phase 4. The results of SCS governed by $SU(4)$ multiplets are displayed in Fig. 7, clearly showing that 2 Kramers-pair are being pumped. Due to the enhanced degeneracy of bound states, the maximum induced electric charge can now oscillate between $0, \pm e$, and $\pm 2e$.

There are many ways to break $U_-(1)$ spin rotation symmetry. For example, we can modify H_j as

$$H_0(\mathbf{k}) \rightarrow H(\mathbf{k}) = H_0(\mathbf{k}) + d_4(\mathbf{k})\Gamma_4 + d_5(\mathbf{k})\Gamma_5, \quad (\text{A3})$$

such that the 2-fold Kramers-degeneracy is preserved. The momentum dependent function $d_4(\mathbf{k}) = t_{d,1}(\cos 2k_x - \cos 2k_y)$ and $d_5(\mathbf{k}) = t_{d,2} \sin k_x \sin k_y$ maintain 4-fold rotation symmetry and also vanish at the time-reversal-invariant momentum points. Following Ref. 26, it can be shown that $\mathfrak{C}_{R,GS}$ and SCS for all phases remain unchanged. But d -wave perturbations destroy *gapless edge-states*. If B_{1g} term is changed to $(\cos k_x - \cos k_y)$, X points cannot participate in band inversion. Thus, states with even integer winding number become trivialized and no longer display SCS and spin-pumping.

An example of decoupled models with higher number of bands can be found in Ref. 23. Using a model of three Kramers degenerate bands on the Kagome lattice, with $U(1)$ spin-rotation symmetry, Wang *et al.* found $(\mathfrak{C}_{R,1}, \mathfrak{C}_{R,2}, \mathfrak{C}_{R,3}) = (-1, +2, -1)$. Consequently, $C_{R,GS} = -1, +1$ for $1/3$ - and $2/3$ - filled insulators, and both states exhibited SCS governed by $SU(2)$ multiplets. This situation is similar to our observations in β -bismuthene.

Therefore, we can conclude that flux tube can perform \mathbb{N} and \mathbb{Z} classification of quantum spin Hall states, irrespective of spin-rotation symmetry. We will further substantiate this conclusion by studying momentum space

topology and real space response of (111)-bilayer of antimony (antimonene) in Sec. C.

Appendix B: Magnitude of relative Chern numbers

Recently, the in-plane Wilson loop has been utilized to quantify magnitude of $SU(2)$ Berry flux of constituent Kramers-degenerate bands of two-dimensional first and higher-order topological insulators.^{26,29} The in-plane Wilson loop of n -th band measures $SU(2)$ Berry phase accrued upon parallel transport along a non-intersecting closed contour C . It is defined by

$$W_n = \mathcal{P} \exp \left[i \oint A_{j,n}(\mathbf{k}) d\mathbf{k}_j \right] = \exp \left(i \theta_n \hat{\Omega}_n \cdot \boldsymbol{\sigma} \right), \quad (\text{B1})$$

where $A_{j,n}^{ss'}(\mathbf{k}) = -i \langle \psi_{n,s}(\mathbf{k}) | \partial_j \psi_{n,s'}(\mathbf{k}) \rangle$ describes components of $SU(2)$ Berry connection, $\partial_j = \frac{\partial}{\partial k_j}$, $\psi_{n,s=\pm 1}(\mathbf{k})$ are degenerate eigenfunctions of n -th band, and \mathcal{P} indicates path-ordering. While the angle θ_n measures gauge-invariant magnitude of non-Abelian flux enclosed by C , the three-component unit vector $\hat{\Omega}_n$ depends on gauge choice.

Following the convention of defining gauge-invariant eigenvalues of Wilson lines or Wannier center charges, we analyze eigenvalues of $\text{Im}(\text{Ln}(W_n)) \equiv \pm |\theta_n| \bmod \pi$. In-plane loops are calculated with Wannier90⁴⁴ and Z2Pack software packages, by following C_3 -symmetry preserving contour, shown in Fig. 8(a). The area enclosed by the contour is systematically increased from zero to the area of first Brillouin zone. The number of winding of θ_n corresponds to the absolute value of relative Chern number $|\mathfrak{C}_{R,n}|$. The results for bands 1-6 are shown in Fig. 8(b)-8(g).

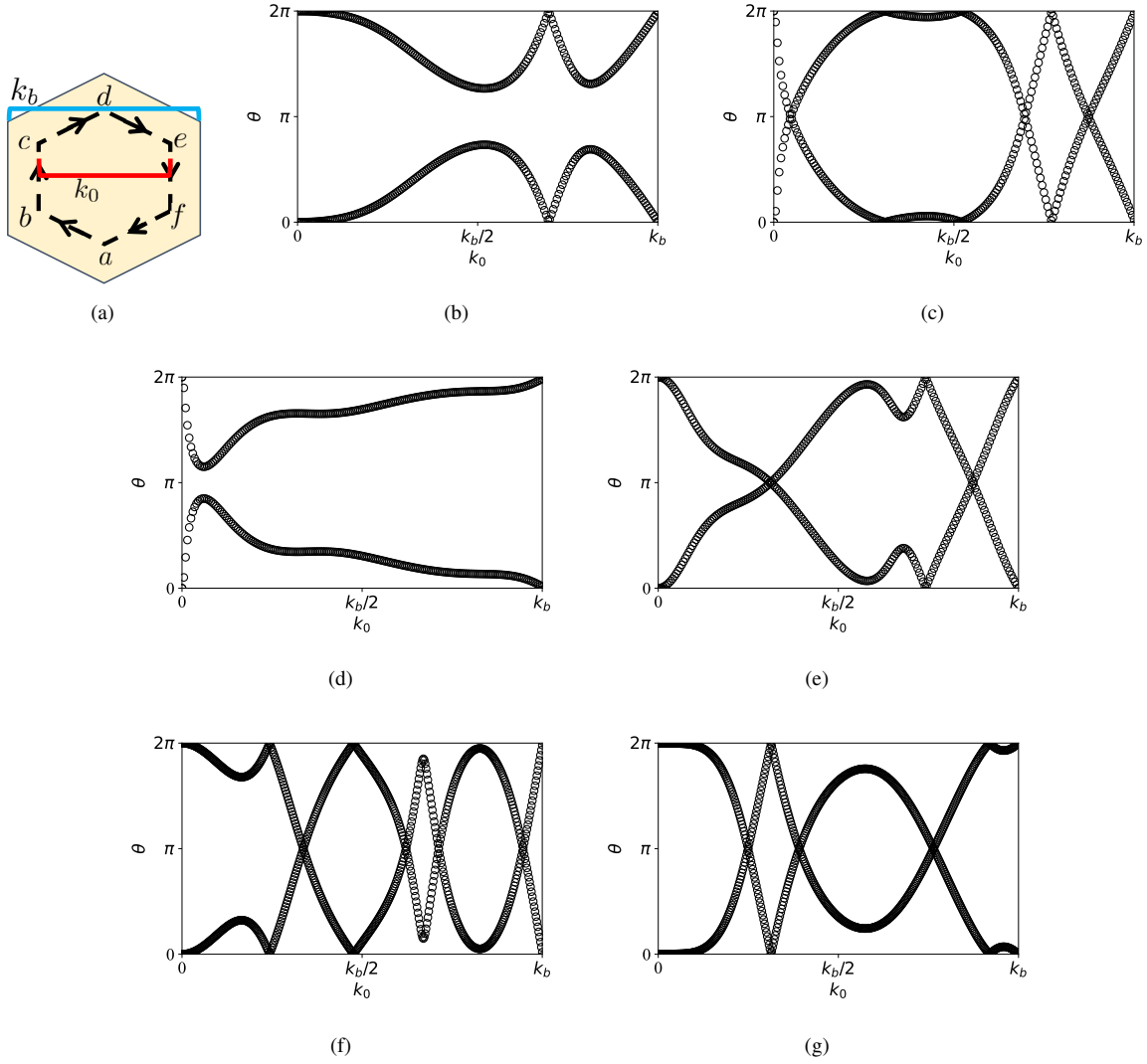


FIG. 8. (a) Schematic of path ($abcdef$) for calculating in-plane Wilson loop. The size k_0 is increased from 0 to k_b . The results for bands 1-6 are shown in (b)-(g), respectively. Trivial bands 1 and 3 do not show winding of θ . For bands 2 and 6, possessing non-trivial \mathbb{Z}_2 index, θ winds once. For \mathbb{Z}_2 -trivial bands 4 and 5, θ winds twice. Therefore, bands 1 through 6 support relative Chern numbers $|\mathcal{C}_{R,n}| = 0, 1, 0, 2, 2, 1$, respectively, as listed in Table I.

Appendix C: Analysis of β -antimonene

In contrast to β -bismuthene, the occupied subspace of single layer of (111) antimony (β -antimonene) supports trivial \mathbb{Z}_2 -classification with $\nu_{0,GS} = 0$. Whether the ground state supports quantum spin Hall effect can be directly addressed by combined analysis of momentum space topology and real-space response. The bulk band structure and \mathbb{N} -classification of constituent bands are shown in Fig. 9(a) and Fig. 9(b), respectively. We have used the lattice parameters given by Mounet *et al.*⁴⁰. Since occupied bands $n = 1, 2, 3$ possess $|\mathcal{C}_{R,n}| = 0, 1, 1$, $|\mathcal{C}_{R,GS}| = 0, 2$ are two possible options for the net relative Chern number.

The first principles calculations show that all three components of spin Hall conductivity vanish for the half-filled insulating state (see Fig. 9(c)). To unambiguously probe topological response, we have performed thought experiments with flux tube for a system size of 24×24 unit cells, under periodic boundary conditions. The spectrum does not show any mid-gap bound states for $N_e = N/2$ and no spin-pumping is observed (see Fig. 9(d)), implying $\mathcal{C}_{R,GS} = 0$. Therefore, $(\mathcal{C}_{R,2}, \mathcal{C}_{R,3}) = \pm(1, -1)$ are the possible assignments of signed relative Chern numbers. Due to the lack of any further direct band gaps, we do not pursue the analysis for other filling fractions.

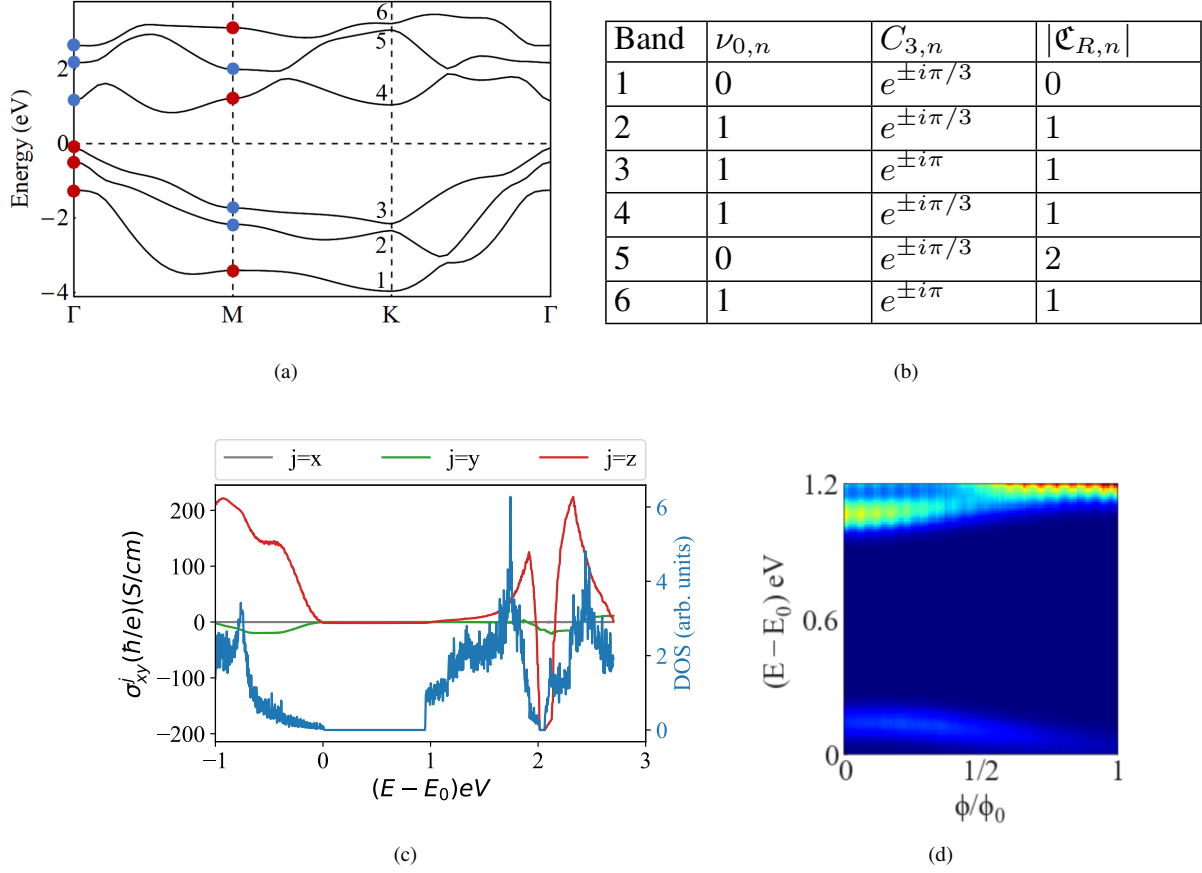


FIG. 9. (a) Band structure of β -antimonene, along high-symmetry path of hexagonal Brillouin zone. The bands are numbered according to their energies at Γ point, and parity eigenvalue $+1$ (-1) at time-reversal-invariant momentum points are denoted by red (blue) dots. (b) Summary of momentum-space topology of constituent bands, where $\nu_{0,n}$, $C_{3,n}$, and $\mathfrak{C}_{R,n}$ respectively denote the \mathbb{Z}_2 index, 3-fold rotation eigenvalue, and the relative Chern number of n -th Kramers-degenerate bands. (c) First principle calculations of spin Hall conductivity. When the Fermi level is tuned inside direct band gap, all three components of spin Hall conductivity vanish for the insulating state. (d) Local density of states on the magnetic flux tube in the vicinity bulk band gap does not show any spin-pumping, which shows that the net relative Chern number $\mathfrak{C}_{R,GS} = 0$.

ACKNOWLEDGMENTS

This work was supported by the National Science Foundation MRSEC program (DMR-1720139) at the Materials Research Center of Northwestern University, and the start up funds of P. G. provided by the Northwestern University. A part of this work was performed at the Aspen Center for Physics, which is supported by National Science Foundation grant PHY-1607611.

- ¹ R. B. Laughlin, “Quantized Hall conductivity in two dimensions,” *Phys. Rev. B* **23**, 5632–5633 (1981).
- ² D. J. Thouless, M. Kohmoto, M. P. Nightingale, and M. den Nijs, “Quantized Hall conductance in a two-dimensional periodic potential,” *Phys. Rev. Lett.* **49**, 405–408 (1982).
- ³ F. D. M. Haldane, “Model for a quantum Hall effect without Landau levels: condensed-matter realization of the parity anomaly,” *Phys. Rev. Lett.* **61**, 2015–2018 (1988).
- ⁴ C. L. Kane and E. J. Mele, “ \mathbb{Z}_2 topological order and the quantum spin Hall effect,” *Phys. Rev. Lett.* **95**, 146802 (2005).
- ⁵ B. A. Bernevig, T. L. Hughes, and S.-C. Zhang, “Quantum spin Hall effect and topological phase transition in HgTe quantum wells,” *Science* **314**, 1757–1761 (2006).
- ⁶ S. Murakami, “Quantum spin Hall effect and enhanced magnetic response by spin-orbit coupling,” *Phys. Rev. Lett.* **97**, 236805 (2006).
- ⁷ M. König *et al.*, “Quantum spin Hall insulator state in HgTe quantum wells,” *Science* **318**, 766–770 (2007).
- ⁸ L. Fu and C. L. Kane, “Topological insulators with inversion symmetry,” *Phys. Rev. B* **76**, 045302 (2007).
- ⁹ R. Roy, “ \mathbb{Z}_2 classification of quantum spin Hall systems: An approach using time-reversal invariance,” *Phys. Rev. B* **79**, 195321 (2009).
- ¹⁰ Qian Niu, D. J. Thouless, and Yong-Shi Wu, “Quantized Hall conductance as a topological invariant,” *Phys. Rev. B* **31**, 3372–3377 (1985).
- ¹¹ R. Yu, X.-L. Qi, B. A. Bernevig, Z. Fang, and X. Dai, “Equivalent expression of \mathbb{Z}_2 topological invariant for band insulators using the non-abelian Berry connection,” *Phys. Rev. B* **84**, 075119 (2011).
- ¹² A. A. Soluyanov and D. Vanderbilt, “Computing topological invariants without inversion symmetry,” *Phys. Rev. B* **83**, 235401 (2011).
- ¹³ A. Alexandradinata, X. Dai, and B. A. Bernevig, “Wilson-loop characterization of inversion-symmetric topological insulators,” *Phys. Rev. B* **89**, 155114 (2014).
- ¹⁴ D. Gresch *et al.*, “Z2pack: Numerical implementation of hybrid Wannier centers for identifying topological materials,” *Phys. Rev. B* **95**, 075146 (2017).
- ¹⁵ D. N. Sheng, Z. Y. Weng, L. Sheng, and F. D. M. Haldane, “Quantum spin-Hall effect and topologically invariant Chern numbers,” *Phys. Rev. Lett.* **97**, 036808 (2006).
- ¹⁶ X.-L. Qi, Y.-S. Wu, and S.-C. Zhang, “General theorem relating the bulk topological number to edge states in two-dimensional insulators,” *Phys. Rev. B* **74**, 045125 (2006).
- ¹⁷ X.-L. Qi, T. L. Hughes, and S.-C. Zhang, “Topological field theory of time-reversal invariant insulators,” *Phys. Rev. B* **78**, 195424 (2008).
- ¹⁸ X.-L. Qi and S.-C. Zhang, “Spin-charge separation in the quantum spin Hall state,” *Phys. Rev. Lett.* **101**, 086802 (2008).
- ¹⁹ Y. Ran, A. Vishwanath, and D.-H. Lee, “Spin-charge separated solitons in a topological band insulator,” *Phys. Rev. Lett.* **101**, 086801 (2008).
- ²⁰ R. Jackiw and C. Rebbi, “Solitons with fermion number $1/2$,” *Phys. Rev. D* **13**, 3398–3409 (1976).
- ²¹ W. P. Su, J. R. Schrieffer, and A. J. Heeger, “Solitons in polyacetylene,” *Phys. Rev. Lett.* **42**, 1698–1701 (1979).
- ²² S. A. Kivelson, D. S. Rokhsar, and J. P. Sethna, “Topology of the resonating valence-bond state: Solitons and high- T_c superconductivity,” *Phys. Rev. B* **35**, 8865–8868 (1987).
- ²³ Z. Wang and P. Zhang, “Quantum spin Hall effect and spin-charge separation in a kagomé lattice,” *New Journal of Physics* **12**, 043055 (2010).
- ²⁴ V. Juričić, A. Mesaros, R.-J. Slager, and J. Zaanen, “Universal probes of two-dimensional topological insulators: Dislocation and π flux,” *Phys. Rev. Lett.* **108**, 106403 (2012).
- ²⁵ A. Mesaros, R.-J. Slager, J. Zaanen, and V. Juričić, “Zero-energy states bound to a magnetic π -flux vortex in a two-dimensional topological insulator,” *Nuc. Phys. B* **867**, 977–991 (2013).
- ²⁶ A. C. Tyner, S. Sur, D. Puggioni, J. M. Rondinelli, and P. Goswami, “Topology of three-dimensional Dirac semimetals and generalized quantum spin Hall systems without gapless edge modes,” *arXiv:2012.12906v2* (2020).
- ²⁷ A. C. Tyner and P. Goswami, “Witten effect and \mathbb{Z} -classification of three-dimensional topological insulators,” *arXiv:2206.10636* (2022).
- ²⁸ W. A. Benalcazar, B. A. Bernevig, and T. L. Hughes, “Quantized electric multipole insulators,” *Science* **357**, 61–66 (2017).
- ²⁹ A. C. Tyner *et al.*, “Quantized non-abelian, Berry’s flux and higher-order topology of Na_3Bi ,” *arXiv:2102.06207* (2021).
- ³⁰ J. C. Y. Teo, L. Fu, and C. L. Kane, “Surface states and topological invariants in three-dimensional topological insulators: application to $\text{Bi}_{1-x}\text{Sb}_x$,” *Phys. Rev. B* **78**, 045426 (2008).
- ³¹ F. Schindler *et al.*, “Higher-order topology in bismuth,” *Nat. Phys.* **14**, 918–924 (2018).
- ³² C.-H. Hsu *et al.*, “Topology on a new facet of bismuth,” *Proc. Natl. Acad. Sci.* **116**, 13255–13259 (2019).
- ³³ L. Aggarwal, Penghao Zhu, T. L. Hughes, and V. Madhavan, “Evidence for higher order topology in Bi and $\text{Bi}_{0.92}\text{Sb}_{0.08}$,” *Nat. comm.* **12**, 1–6 (2021).
- ³⁴ M. Wada, S. Murakami, F. Freimuth, and G. Bihlmayer, “Localized edge states in two-dimensional topological insulators: Ultrathin Bi films,” *Phys. Rev. B* **83**, 121310 (2011).
- ³⁵ I. K. Drozdov *et al.*, “One-dimensional topological edge states of bismuth bilayers,” *Nat. Phys.* **10**, 664–669 (2014).
- ³⁶ S. Ito *et al.*, “Proving nontrivial topology of pure bismuth by quantum confinement,” *Phys. Rev. Lett.* **117**, 236402 (2016).
- ³⁷ F. Reis *et al.*, “Bismuthene on a SiC substrate: A candidate for a high-temperature quantum spin Hall material,” *Science* **357**, 287–290 (2017).
- ³⁸ M. Bieniek, T. Woźniak, and P. Potasz, “Stability of topological properties of bismuth (1 1 1) bilayer,” *J. Condens. Matter Phys.* **29**, 155501 (2017).
- ³⁹ A. Takayama, T. Sato, S. Souma, T. Oguchi, and T. Takahashi, “One-dimensional edge states with giant spin splitting in a bismuth thin film,” *Phys. Rev. Lett.* **114**, 066402 (2015).
- ⁴⁰ N. Mounet *et al.*, “Two-dimensional materials from high-throughput computational exfoliation of experimentally known compounds,” *Nat. nanotechnol.* **13**, 246–252 (2018).
- ⁴¹ P. Giannozzi *et al.*, “Quantum espresso: a modular and open-source software project for quantum simulations of materials,” *J. Phys. Condens. Matter* **21**, 395502 (19pp) (2009).

- ⁴² P. Giannozzi *et al.*, “Advanced capabilities for materials modelling with quantum espresso,” *J. Phys. Condens. Matter* **29**, 465901 (2017).
- ⁴³ P. Giannozzi *et al.*, “Quantum espresso toward the exascale,” *J. Chem. Phys.* **152**, 154105 (2020).
- ⁴⁴ G. Pizzi *et al.*, “Wannier90 as a community code: new features and applications,” *J. Phys. Condens. Matter* **32**, 165902 (2020).
- ⁴⁵ M. P. Lopez Sancho, J. M. Lopez Sancho, J. M. L. Sancho, and J. Rubio, “Highly convergent schemes for the calculation of bulk and surface Green functions,” *J. Phys. F: Met. Phys.* **15**, 851 (1985).
- ⁴⁶ Q. S. Wu, S. N. Zhang, H.-F. Song, M. Troyer, and A. A. Soluyanov, “WannierTools : An open-source software package for novel topological materials,” *Computer Physics Communications* **224**, 405 – 416 (2018).
- ⁴⁷ J. Qiao, J. Zhou, Z. Yuan, and W. Zhao, “Calculation of intrinsic spin Hall conductivity by Wannier interpolation,” *Phys. Rev. B* **98**, 214402 (2018).
- ⁴⁸ D. Destrz *et al.*, “Magnetism and anomalous transport in the Weyl semimetal PrAlGe: possible route to axial gauge fields,” *npj Quantum Mater.* **5**, 1–8 (2020).
- ⁴⁹ S. S. Tsirkin, “High performance Wannier interpolation of Berry curvature and related quantities with WannierBerri code,” *npj Computational Materials* **7**, 1–9 (2021).
- ⁵⁰ G. Rosenberg and M. Franz, “Witten effect in a crystalline topological insulator,” *Phys. Rev. B* **82**, 035105 (2010).